Original paper

Folia Neuropathologica

Construction of a diagnostic model for ischemic stroke based on immune-related genes

Yingfeng Weng[1*], Bin Liu[2*], Zhibin Chen[1], Yangbo Hou[1], Dan Wu[3], Lin Ma[4], Guoyi Li[1]

[1]Department of Neurology, Putuo Hospital, Shanghai University of Traditional Chinese Medicine, Shanghai, China, [2]Department of Neurology, Shanghai Shuguang Hospital, Shanghai University of Traditional Chinese Medicine, Shanghai, China, [3]Department of Radiology, Putuo Hospital, Shanghai University of Traditional Chinese Medicine, Shanghai, China, [4]Department of Interventional Radiology, Shanghai Tongji Hospital, Tongji University School of Medicine, Shanghai, China

[*] *These authors contributed equally to this work.*

Folia Neuropathol 2024; 62 (2): 171-186 *DOI: https://doi.org/10.5114/fn.2024.135846*

Abstract

Introduction: *This study aimed to screen immune-related marker genes of ischemic stroke (IS).*
Material and methods: *Two IS-related gene expression datasets were downloaded. The significantly differentially expressed genes (DEGs) and miRNAs (DEMs) between IS and control groups were selected. The differential immune cells were analysed. Weighted gene co-expression network analysis (WGCNA) was applied to analyse immune-related genes, followed by function analysis and interaction network construction. Then, key genes were further screened using optimization algorithm to construct a diagnostic model. Finally, miRNA regulatory network of several key genes was established.*
Results: *In total 321 DEGs and 140 DEMs were obtained. 11 immune cell types were significantly different between IS and control groups. WGCNA identified two key modules, involving 202 differential immune genes. The greenyellow module was enriched in biological processes and pathways associated with T cells, while the midnightblue module was mainly associated with apoptosis, and inflammatory response-related functions and pathways. Protein interaction network identified 10 hub nodes, such as CD8A, ITGAM and TLR4. LASSO regression selected 8 key feature genes, and a risk score model was established. Key model genes were enriched in 63 GO biological processes, such as microglial cell activation, and B cell apoptotic process, and 3 KEGG pathways, such as negative regulation of nuclear cell cycle DNA replication, and hematopoietic cell lineage. Finally, a total of 25 miRNA-target relationship pairs were obtained.*
Conclusions: *This study identified some immune-related marker genes and constructed a diagnostic model based on 8 immune-related genes in IS.*

Key words: *ischemic stroke, gene, immune, diagnostic model.*

Introduction

Stroke is a leading cause of disability around the world. Ischemic stroke (IS) accounts for more than 80% of stroke cases. IS usually results from sudden interruption of blood flow and decreased oxygen levels in the brain [8], which can trigger a complex chain of neurological events including calcium overload, oxidative stress, excitotoxicity, apoptosis and inflammation, resulting in focal brain damage [10]. Nowadays, with

Communicating authors:
Guoyi Li, Department of Neurology, Putuo Hospital, Shanghai University of Traditional Chinese Medicine, 164 Lanxi Road, Shanghai, China, phone: 86-021-22233222, e-mail: shptstxd@163.com
Lin Ma, Department of Interventional Radiology, Shanghai Tongji Hospital, Tongji University School of Medicine, 389 Xincun Road, Shanghai, China, phone: 86-021-56051080, e-mail: marin2012@126.com
Received: 28.11.2022, **Accepted:** 12.05.2023, **Online publication:** 28.06.2024

the prevalence of unhealthy lifestyles and exposure to cardiovascular risk factors, the burden of IS is rapidly increasing [1]. As a result, the early diagnosis and treatment of IS faces huge challenges.

A growing number of studies have demonstrated that neuroinflammation, including circulating immune cells infiltration, microglia activation, and upregulation of pro-inflammatory cytokines plays a key role in stroke-induced brain damage [9,18,35]. Specially, infiltration of inflammatory cells can stimulate strong immune response and lead to immune micro-environment dysfunction in the central nervous system, further aggravating IS [20]. Currently, it has been proposed that immunomodulation could delay the progression of IS, and improve the neurological function [12,13]. Therefore, immunoregulatory therapy as an alternative to traditional therapy is worthy of further study. Whereas, systematic studies on the distribution of peripheral blood immune cell subtypes and immune-related gene modules in IS patients are still limited.

This study was designed to screen immune-related marker genes of IS based on the gene sequencing datasets (GSE16561 and GSE22255) obtained from the Gene Expression Omnibus (GEO). The BP terms and KEGG pathway enrichment analyses of key model genes were constructed. Additionally, a diagnostic model was established with the immune-related genes. The findings of this study could provide a reliable theoretical basis for the diagnosis of IS and the target of immunotherapy.

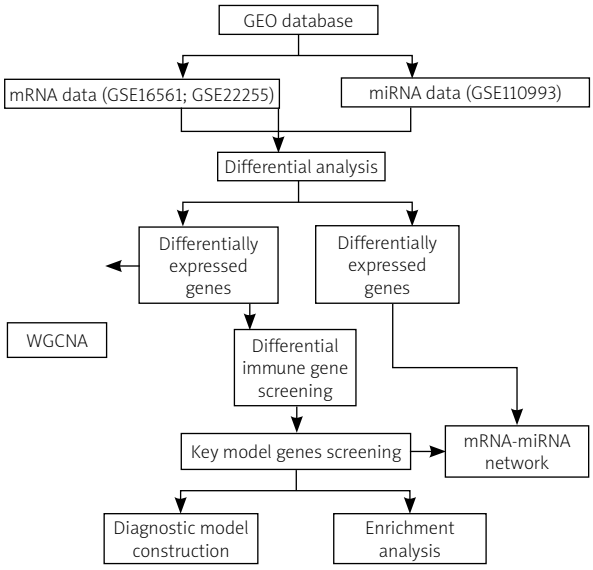

Fig. 1. Algorithm flowchart

Material and methods

Data download

Ischemic stroke-related dataset GSE16561 was downloaded from the NCBI GEO [2] database, which included peripheral blood tissue samples from 39 patients with IS and 24 normal controls. GPL6883 Illumina HumanRef-8 v3.0 expression BeadChip platform was used for gene chip determination. This dataset was used as a training set.

Another dataset GSE22255 was also downloaded from the GEO database. The peripheral blood mononuclear cell tissue samples of 20 patients with IS and 20 normal controls were selected. GPL570 [HG-U133_Plus_2] Affymetrix Human Genome U133 Plus 2.0 Array platform was used for microarray determination. The dataset was mainly used to validate the diagnostic model (Fig. 1).

Additionally, the miRNA high-throughput sequencing data of IS, GSE110993 including 20 IS patients and 20 matched healthy control subjects, were downloaded from the GEO database. Here, the miRNA result files were directly downloaded after DESeq2 pre-processing and differential analysis for subsequent analysis.

Data pre-processing

For the above two gene chip datasets (GSE16561 and GSE22255), the probe expression matrixes after pre-processing, standardization and log2 transformation were obtained from the GEO database, and then the annotation file of the platform was downloaded. The probes that did not match the gene symbol were deleted by one-by-one matching between the probe number and the gene symbol. We took the mean value of different probes as the expression value of this gene for subsequent analysis.

Differentially expressed genes (DEGs) and miRNAs (DEM) screening

Based on the analysis dataset, the classical Bayesian method in limma 3.10.3 [31] was used to analyse the differentially expressed genes (DEGs) of IS vs. normal controls. The p value and log FC value were adjusted with BH method. The differential expression thresholds were adj. p value < 0.05 and |logFC| > 0.585.

For miRNA data, we directly set the threshold based on the miRNA result file. The differentially expressed miRNAs (DEMs) with $p < 0.05$ and |logFC| > 0.585 were regarded as significant DEMs. Volcano plots were used for visualization display of DEGs and DEMs, respectively.

Immune infiltration analysis

To study the infiltration of immune cells in IS and normal controls, the CIBERSORT algorithm [4] and LM22 gene set were used to calculate the infiltration ratio of 22 kinds of immune cells in samples of GSE16561 dataset. Then, according to the grouping of samples, Wilcoxon test was applied to calculate the significance p value of each immune cell between IS and normal controls, and cells with $p < 0.05$ were retained for the following analysis.

Screening of immune cell-related genes through weighted gene co-expression network analysis (WGCNA)

Weighted gene co-expression network analysis (WGCNA) is used for the analysis of gene expression patterns of samples, which could cluster genes with similar expression patterns, and distinguish modules through gene expression similarity. Then, the correlations between the modules, and between the module and samples were calculated to screen highly relevant modules, and analyse the genes in the module to find the target genes relevant to the study.

To find out the module genes highly related to differential immune cells in GSE16561, we first ranked all genes in the dataset according to the variance from the largest to the smallest. Then, the genes with the top 25% of variance were selected for analysis using R package WGCNA [21] (version 1.61) based on the above differential immune cells as traits.

During WGCNA, the elements of the defined gene co-expression matrix are the weighted values of gene correlation coefficients, and the selection criterion of the weights is to make the connections among genes in the network following scale-freenetworks. Here, the weighted value is "softPower". Firstly, by setting a series of powers, the square of correlation coefficient between the connectivity degree k and p(k) and the average connectivity degree under each power were calculated, and then the appropriate power value was selected. Secondly, with clustering and dynamic pruning method, the parameters (minModuleSize = 50; MEDissThres = 0.3) were set to cluster the highly correlated genes into modules. The correlation between modules and phenotype (infiltration level of differential immune cells) was finally calculated. The modules with correlation coefficient > 0.5 and $p < 0.05$ were closely related to immunity.

Differential immune gene screening and analysis

The intersection genes of immune cell-related genes and DEGs were obtained, and the function analysis and PPI network analysis were conducted based on the differential immune genes.

Based on the differential immune genes obtained above, Gene Ontology (GO) biological process (BP) [1] and pathway [17] enrichment analyses were carried out respectively using the online tool DAVID [30], and the number of enriched genes was at least 2.

To understand the protein interactions between the differential immune genes obtained above, the online database STRING [27] (version 11.0) was used to predict and analyse the interaction relationship between the gene-encoded proteins. Protein-protein interaction (PPI) score was set to be 0.4. In addition, the topological properties of nodes were analysed using CytoNCA [34] plug-in 2.1.6, including "degree", "betweenness" and "closeness". The top 10 intersection genes ranked by topological properties were selected as hub genes.

Key genes screening and diagnostic model construction

Based on the hub genes, LASSO algorithm was used to screen feature genes. Then, glmnet package version 4.0-2 [15] in R 3.6.1 was used for regression analysis of the hub genes preliminarily screened, and the parameter was set to be: nfold = 20 (20-fold cross-validation). The following formula was further used for model construction:

$$\text{Risk score (RS)} = \Sigma\, \beta_{gene} \times Exp_{gene}$$

Where β_{gene} represents the LASSO regression coefficient of each gene, and Exp_{gene} represents the expression of the gene in each sample.

After obtaining RS, the median value was used as the critical value, and the samples were divided into high- and low-risk groups for subsequent analysis.

Furthermore, in order to verify whether the model had a diagnostic value, GSE22255 was used for validation. Briefly, the expression levels of model genes in each sample of GSE22255 were extracted, and the same formula was used to construct the model in combination with the LASSO regression coefficient obtained above. The ROC curve was drawn and combined with the grouping information of samples.

Evaluation of diagnostic efficacy of key genes

For the key genes obtained from the above analysis, the data of the training set and validation set were used for expression verification, respectively. The expression values of key genes in the data set were extracted, and then combined with the sample grouping, the significance of gene expression differences was calculated

by *t*-test. The expression distribution box diagram was drawn. Moreover, the diagnostic ROC curves of key genes were drawn in the training set and validation set.

Enrichment analysis of key model genes

The BP terms and Kyoto Encyclopedia of Genes and Genomes (KEGG) pathways enriched by the key model genes were analysed using ClueGO plug-ins [3] (version 2.5.9) in Cytoscape software [19] (version 3.4.0). The significant threshold was p value < 0.05. Cytoscape software was used to visualize the enrichment results.

miRNA regulatory network construction

Based on the model genes obtained above, we used miRWalk 3.0 [32] database for miRNA prediction, and then took the intersection of the predicted miRNA and the DEMs obtained by the previous screening. The mRNA-miRNA regulatory relationships were visualized using Cytoscape software.

Results

Data pre-processing and differential expression analysis

According to the method, the two sets of gene expression microarray data were firstly downloaded, pre-processed and annotated to obtain the expression matrix.

According to the thresholds, 247 up- and 74 down-regulated DEGs were obtained. Additionally, 11 up- and 129 down-regulated DEMs were obtained. The differential volcano plots of DEGs and DEMs are shown in Figure 2A. As presented in the volcano plots, the DEGs and DEMs of the two groups could be significantly separated.

Immune infiltration analysis

The infiltration ratio of 22 immune cell types in all samples of dataset GSE16561 was calculated, as shown in Figure 2B. Additionally, 11 immune cell types were significantly different between the two groups, including T cells CD8, B cells naïve, T cells CD4 memory activated, T cells follicular helper, T cells regulatory (Tregs), T cells γδ, etc. (Fig. 2C).

Screening of immune cell-related genes with WGCNA

WGCNA analysis was based on GSE16561 gene expression data, and a soft threshold of 6 was selected (Fig. 3A). Then, the modules with correlation coefficient > 0.7 and dissimilarity coefficient < 0.3 were merged and finally integrated into four modules (Fig. 3B). Further, by calculating the correlation between the feature vector gene of each module and phenotype, the correlations between the MEgreenyellow module and T cells CD8, as well as the MEmidnightblue module and macrophages M0 and neutrophils were all over 0.5 (Fig. 3C). Therefore, the two modules were considered as the key modules for the subsequent analysis.

Differential immune gene identification and function and pathway enrichment analysis

The intersection of immune cell-related module genes and DEGs obtained above was taken. As shown in Figure 4A, 76 differential immune genes from the greenyellow module and 126 differential immune genes from the midnightblue module were obtained.

Enrichment analyses of 76 differential immune genes from the greenyellow module and 126 differential immune genes from the midnightblue module, respectively were made. The top 10 items are presented in Figure 4B-E. Briefly, the greenyellow module was enriched in biological processes and pathways related to T cells, while the midnightblue module was associated with inflammatory response, apoptosis, and atherosclerosis.

Protein interaction network and correlation analysis

STRING was used to predict the interaction relationship between the above-mentioned differential immune gene proteins, and 144 proteins and 523 interaction relationship pairs were predicted, as shown in Figure 5. These genes directly interacted closely with each other. Additionally, the top 20 nodes of each topological property were taken and the intersection was identified, obtaining 10 nodes, including CD8A, ITGAM, TLR4, CD19, SELL, TLR2, FCGR1A, CD163, FOS and BCL6.

Key genes screening and diagnostic model construction

LASSO regression analysis was carried out on the 10 hub genes obtained above, and 8 key feature genes including *CD16*, *CD19*, *CD8A*, *FCGR1A*, *BCL6*, *FOS*, *ITGAM* and *TLR2* were obtained (Fig. 6A). The risk score (RS) model was then constructed by combining the above 8 genes and corresponding regression coefficients (Fig. 6B). According to the ROC curve, the AUC was above 0.9, indicating that the model had a good effect on disease prediction (Fig. 6C). In order to verify the prediction effect of the model, an RS model was constructed in GSE22255. As shown in Figure 6D,

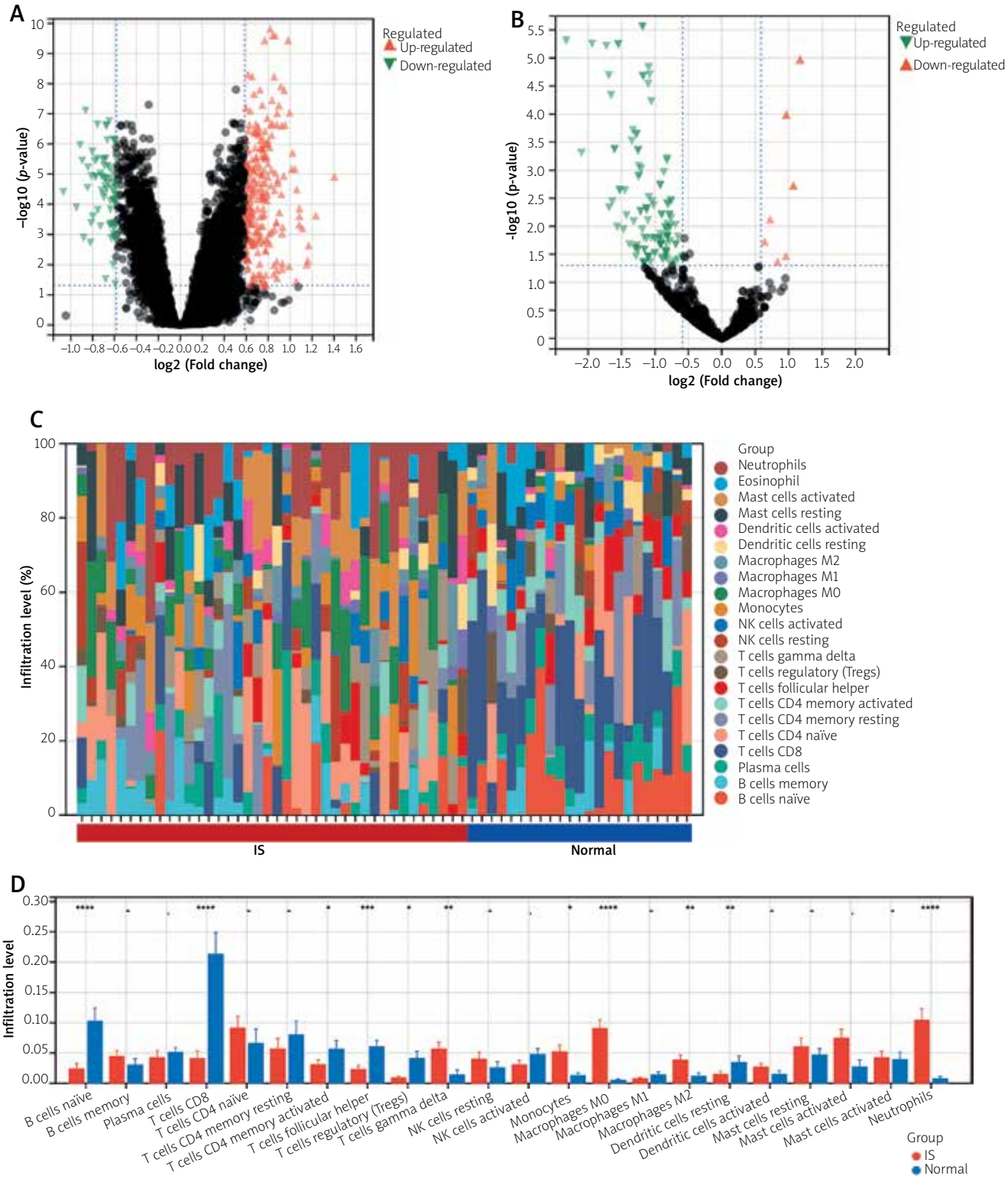

Fig. 2. A, **B**) Volcano maps of differentially expressed genes (**A**) and miRNAs (**B**) (green represents down-regulation, red represents up-regulation, and black represents non-significant genes). **C**) Landscape map of infiltration level distribution proportion of 22 kinds of immune cells in each sample. **D**) Bar charts of the infiltration levels of 22 types of immune cells in disease and control groups.

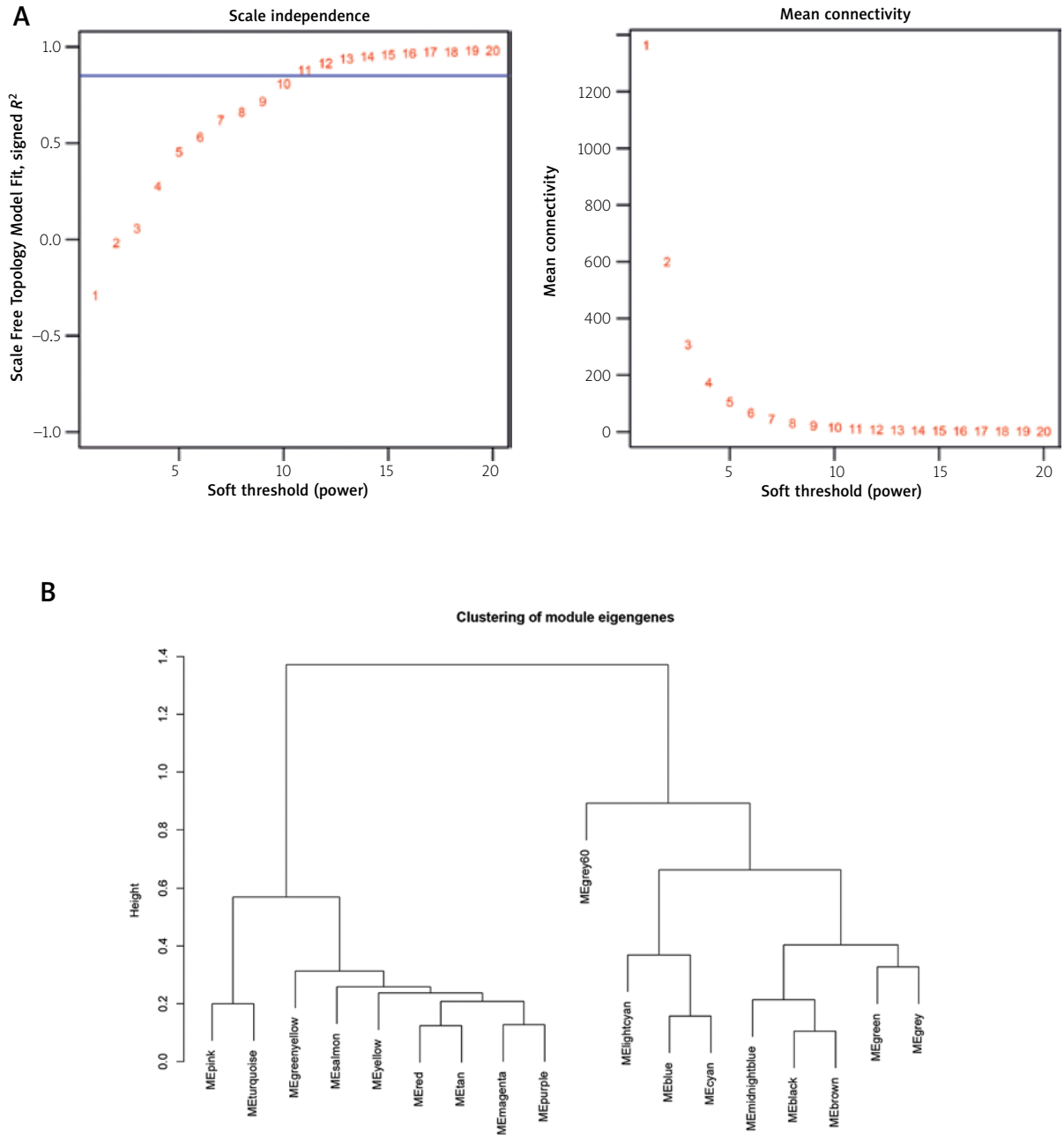

Fig. 3. A) WGCNA power value result. Left: The ordinate represents the square value of the correlation coefficient of the connection degree k and p(k). The higher the square of the correlation coefficient is, the closer the network is to the distribution of the scale-free network. Right: The ordinate represents average connectivity. **B**) WGCNA module clustering and merging results. Module clustering results. The vertical axis shows the different coefficients.

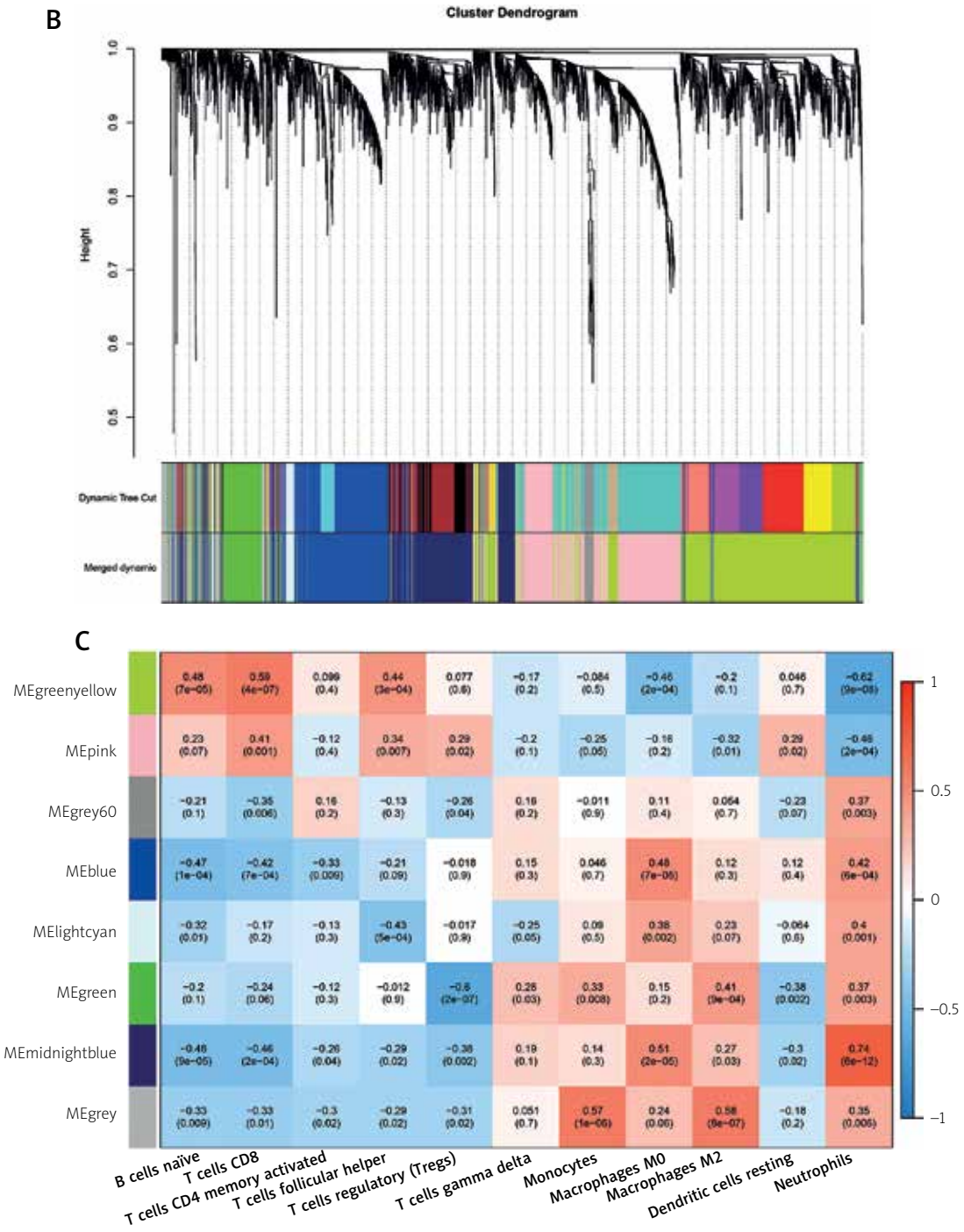

Fig. 3. Cont. **B**) WGCNA module clustering and merging results. Gene modules generated by systematic clustering tree and dynamic shear method. Different colours represent different gene modules in the figure. **C**) Correlation analysis between WGCNA module and differential immune cells. The top number indicates the correlation coefficient, while the bottom number indicates the significance value.

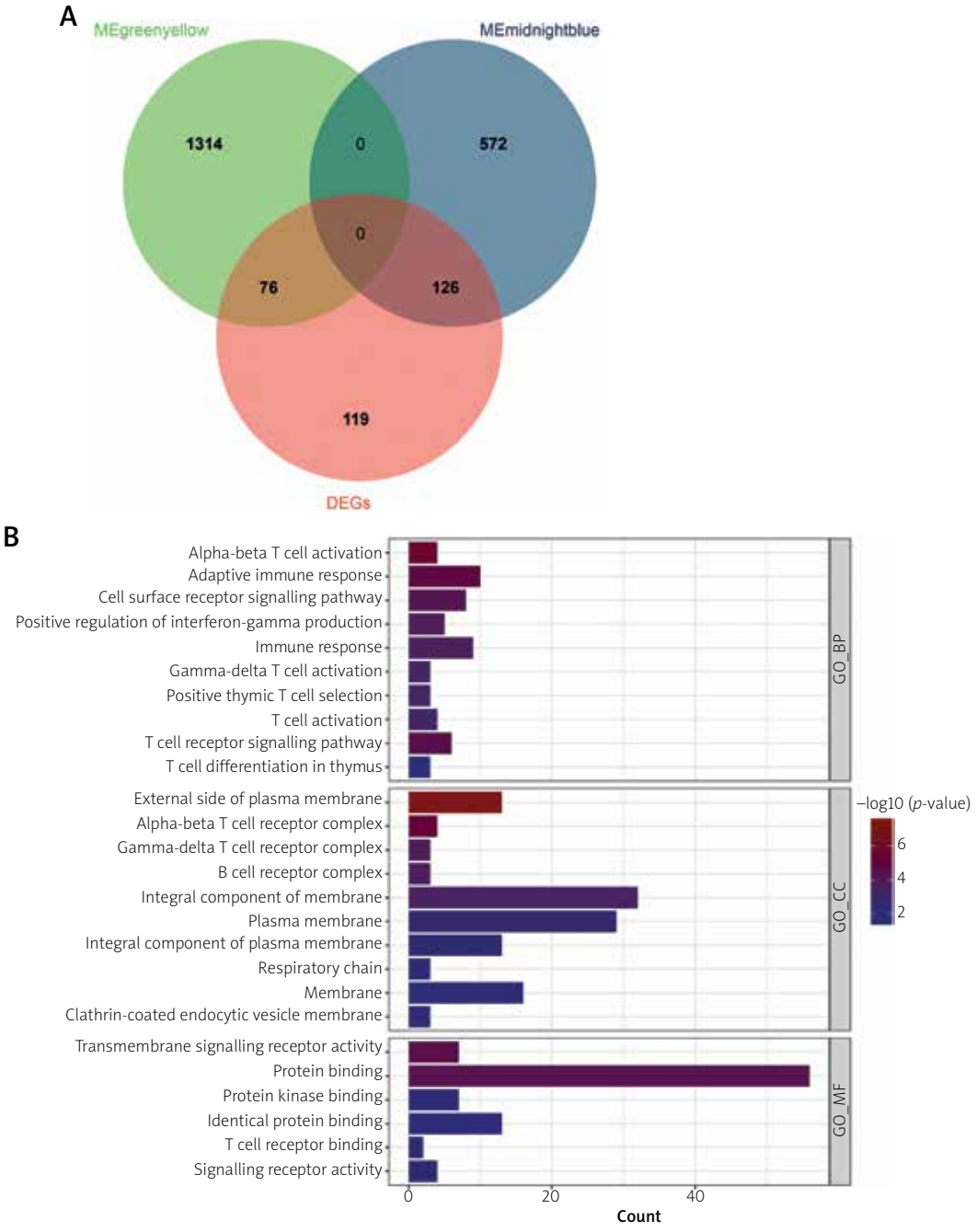

Fig. 4. A) The intersection Venn diagram of differentially expressed genes and immune cell related module genes. **B**) Top 10 results of GO enrichment of differential immune genes in the greenyellow module.

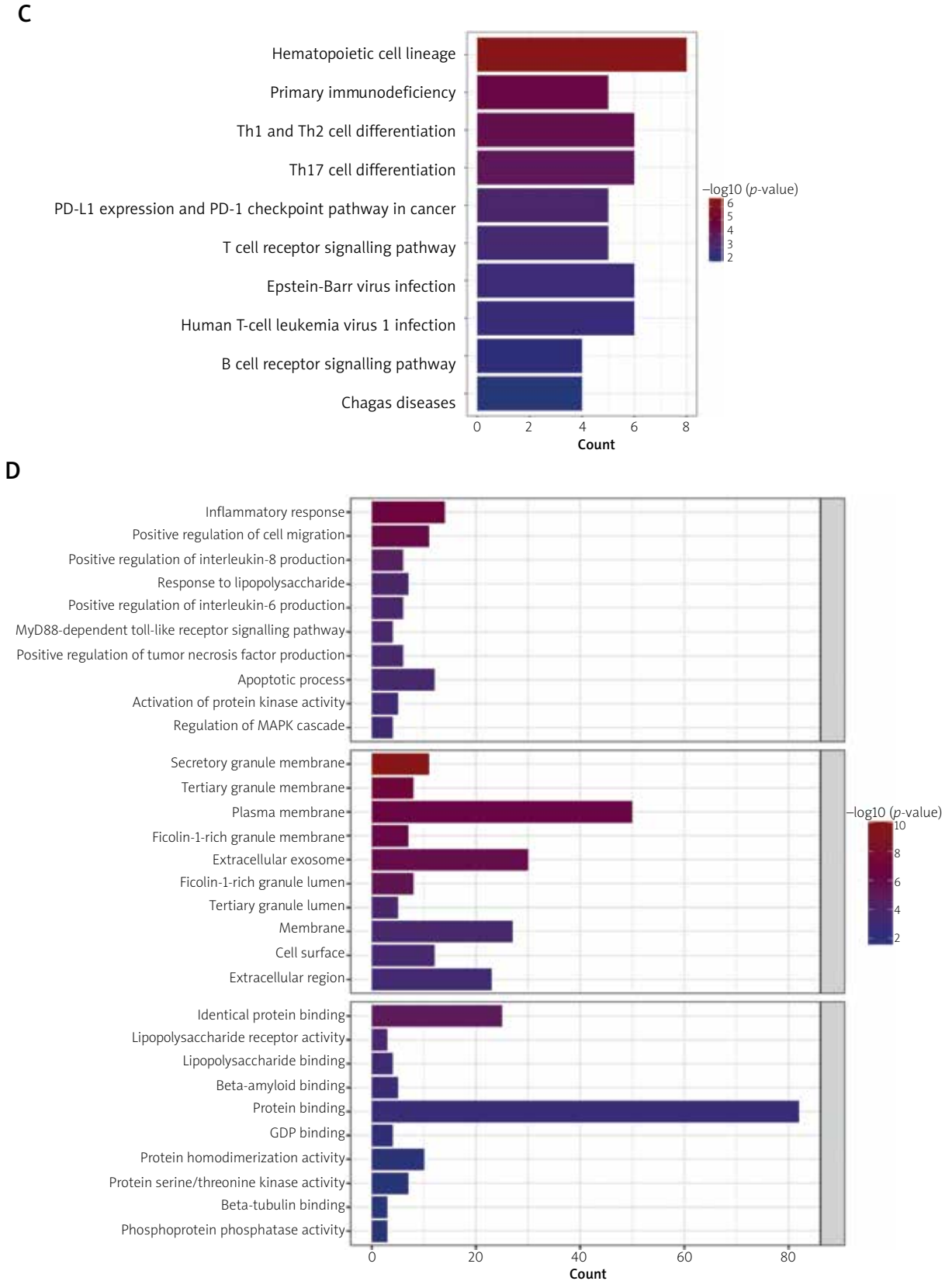

Fig. 4. Cont. **C**) Top 10 results of KEGG pathway enrichment of differential immune genes in the greenyellow module. **D**) Top 10 results of GO enrichment of differential immune genes in midnightblue module.

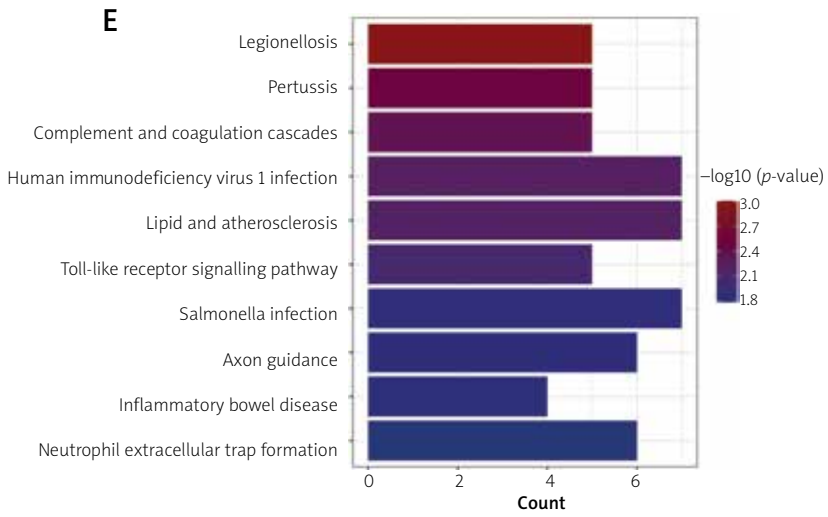

Fig. 4. Cont. **E**) Top 10 results KEGG pathway enrichment of differential immune genes in midnightblue module.

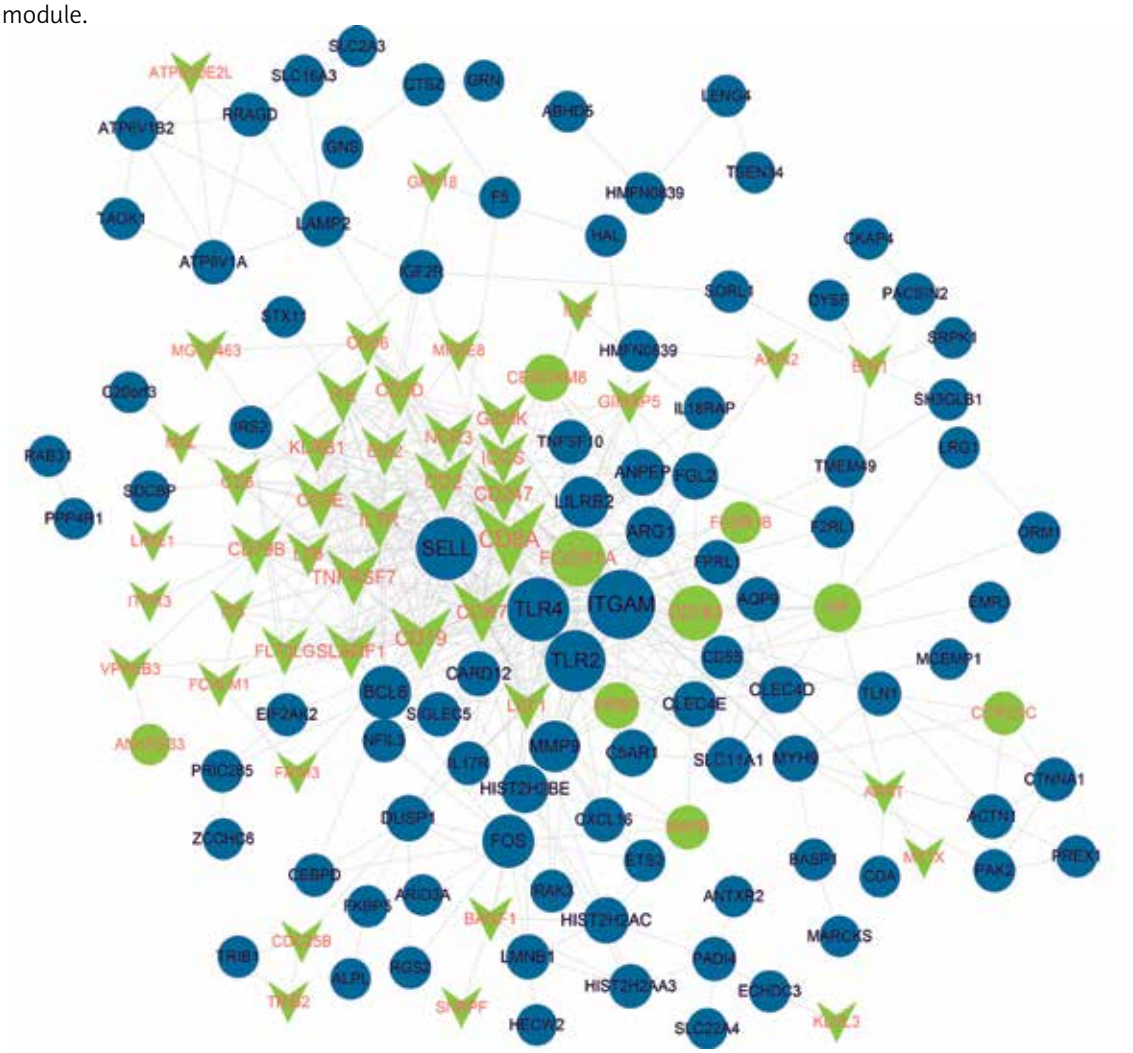

Fig. 5. Protein interaction network constructed by differential immune gene proteins (round represents up-regulated genes, inverted arrow represents down-regulated genes, and different colours represent different modules).

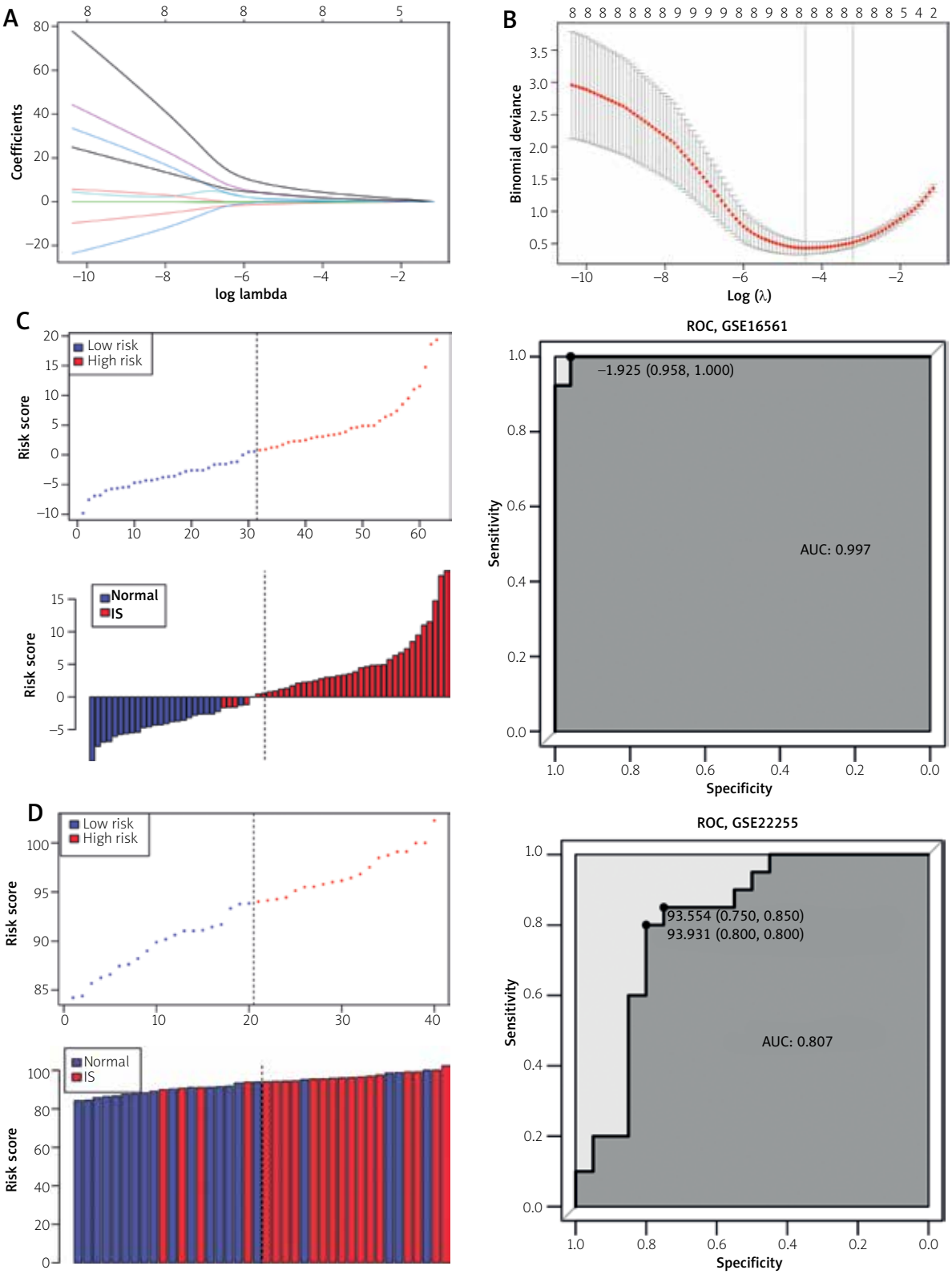

Fig. 6. A, B) LASSO regression process parameter diagram. **A**) The vertical coordinate is the coefficient of variables, and the horizontal coordinate is log(Lambda). With the change of lambda, the coefficient of most variables is finally compressed to 0. **B**) The two dotted lines indicate two special lambda values. **C, D**) Left: Risk score distribution; Right: Predictive ROC curve of the model for disease occurrence in GSE16561 (**C**) and GSE22255 (**D**).

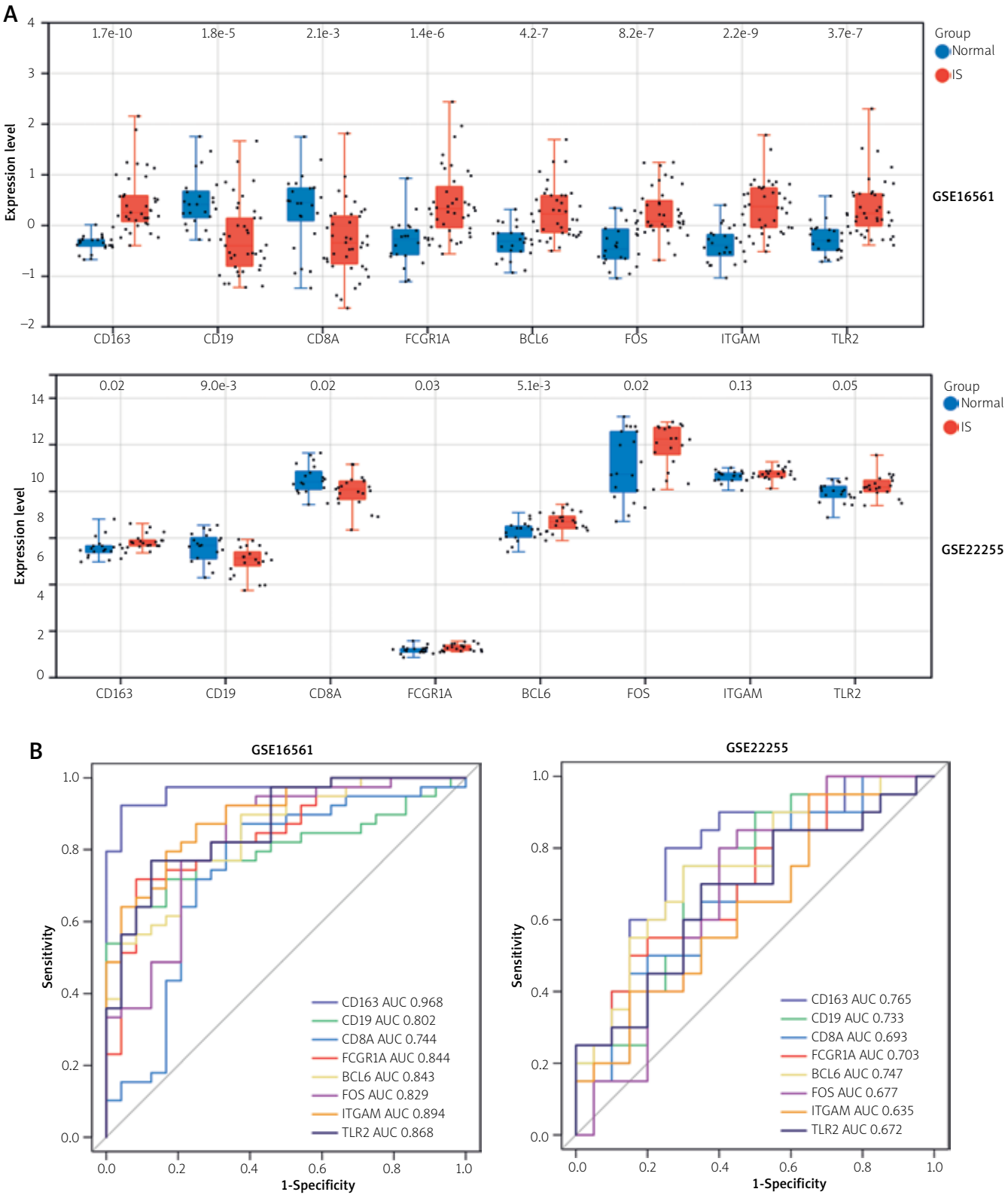

Fig. 7. A) Expression box diagrams of 8 key genes in the training set (top) and validation set (bottom). **B**) ROC curves of 8 key genes in the training set (left) and validation set (right).

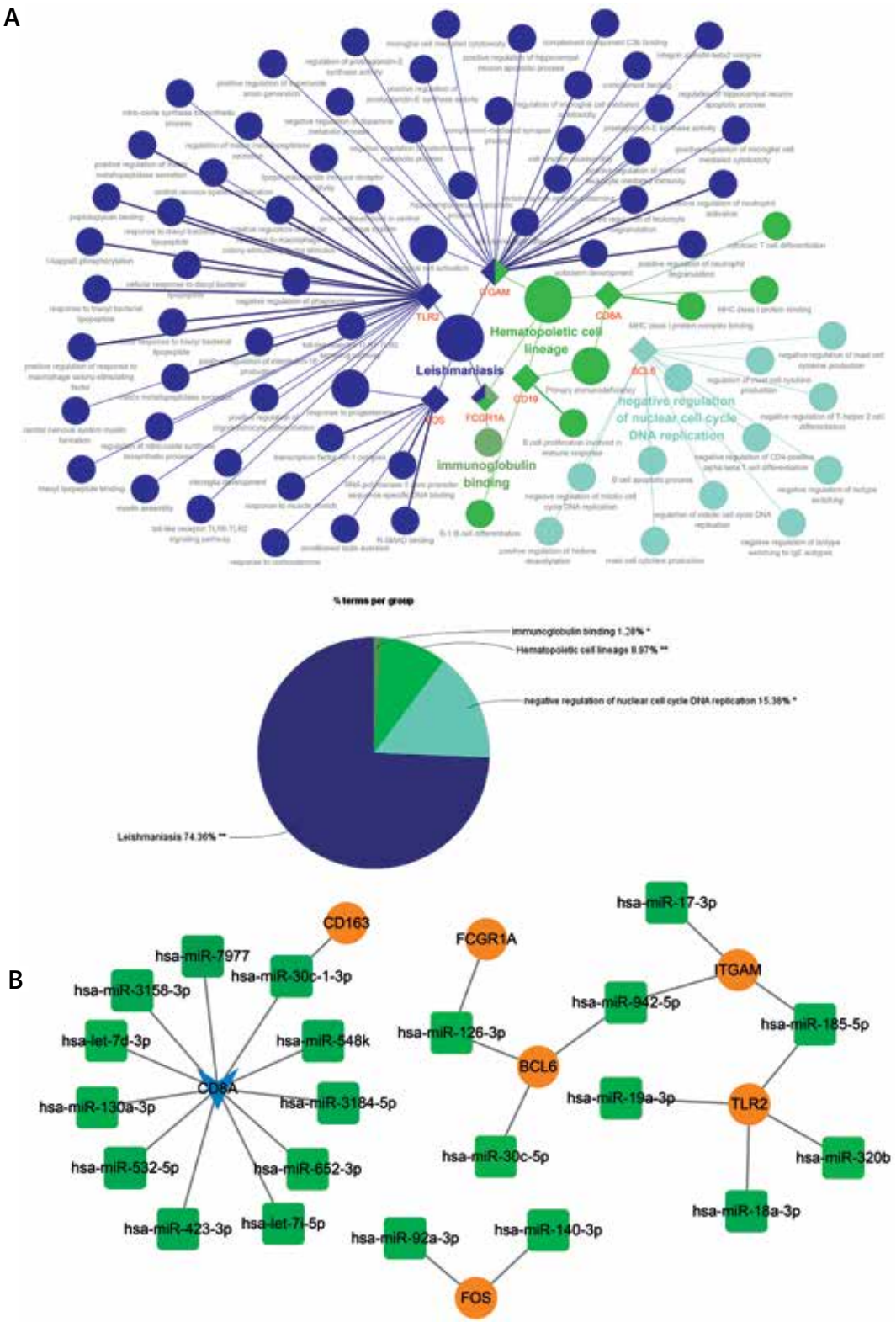

Fig. 8. A) Visualization results of GO BP and KEGG pathway enriched in key model genes (top: Gene-functional network diagram. Diamonds represent genes, circles represent GO BP or KEGG pathway, and different colours represent different functional clusters; bottom: The proportion of each functional cluster). **B**) The miRNA-target regulatory network (yellow circle represents up-regulated gene, blue inverted arrow represents down-regulated gene, green square represents differentially down-regulated miRNA, and darker colour indicates more down-regulated).

the AUC was above 0.8, which indicated that the prediction effect of the model was good.

Evaluation of diagnostic efficacy of key genes

As described in the method, the expression box diagrams of 8 model genes in the training and validation set were respectively drawn, as shown in Figure 7A. The training set was consistent with the validation set for the expression trend of 8 genes. Except for *ITGAM* and *TLR2* that did not reach the significant level in the validation set, the other genes all reached significant differences.

In addition, the diagnostic ROC curves of the 8 key genes are presented in Figure 7B. The diagnostic AUC in the training set was above 0.7, and in the validation set was above 0.6, proving that they had a good diagnostic effect.

GO and KEGG enrichment analyses of key model genes

As shown in Figure 8A, a total of 63 GO biological processes, such as conditioned taste aversion, microglial cell activation, and B cell apoptotic process, as well as 3 KEGG pathways, including Leishmaniasis, negative regulation of nuclear cell cycle DNA replication, and hematopoietic cell lineage.

miRNA regulatory network construction of key genes

miRNA prediction was performed on the above 8 key genes, and the intersection of predicted miRNAs and differentially expressed miRNAs was further obtained. Finally, 25 miRNA-target pairs were obtained, including 7 key model genes and 21 differentially expressed miRNAs. The miRNA-target network was constructed as shown in Figure 8B.

Discussion

Ischemic stroke is a chronic disease that mainly affects cerebral blood vessels. More and more studies have shown that the direct and indirect immune inflammatory responses induced by IS play a key role in the prognosis of cerebral vascular disease [11,26]. In this study, we focused on immune-related marker genes in IS and constructed a diagnostic model based on 8 immune-related genes through WGCNA, which could provide a reliable theoretical basis for the diagnosis of IS and the target of immunotherapy.

Following acute stroke, a variety of immune cells enter the brain parenchyma. In the early stage after stroke, microglia began to increase, and within 1 day after stroke, macrophages, monocytes, myeloid dendritic cells, and neutrophils appeared and lasted until seven days after stroke. Additionally, T and B cells were also detected to have a small increase [6,25]. These immune cells have played important roles in the regulation of the progression of IS [14]. In this study, 11 immune cell types were significantly differential between IS and normal controls, and these immune cells included the cells mentioned above. Therefore, immune cells can not only participate in neuroinflammatory processes, but also maintain the homeostasis of the central nervous system.

On the basis of the differential immune cells, 202 immune-related genes were selected through WGCNA, which were involved in T cell, apoptosis, and inflammatory response related functions and pathways. T cells are important immune cells that participate in the nosogenesis of nervous system diseases *via* the induction of the innate and adaptive immune responses. Following stroke, the T cells migrate to the lesion edge preferentially, increase in number after some days, and can be identified in the brain parenchyma up to 30 days after ischemia [33]. It has been reported that cell death and inflammation are two key biological processes in physiology and pathology [41]. Apoptosis may be an important cause of neuron death after acute brain ischemia, and brain ischemia may lead to IS [28]. Inflammation usually begins in the acute phase of IS and may become the dominant injury mechanism within hours and persist for days [23,40]. Therefore, modulating the inflammatory component may be a therapeutic option for IS.

Presently, several models have been proposed for the diagnosis of stroke. For instance, Laskowitz *et al*. [22] presented a logistic model for the diagnosis of acute stroke. Lu *et al*. [24] developed a Bayesian framework for the construction of a high-confidence syndrome predictor. Different from the models above, our study constructed the model based on the immune-related gene, and 8 genes were finally selected after LASSO regression analysis, and a diagnostic model was established. The AUC of ROC curves was more than 0.8, indicating a good prediction performance for the model. The model genes have also been associated with IS. For example, the c-Fos level was found to significantly increase following experimental cerebral ischemia [36]. *BCL6* has been previously reported to attenuate inflammation [5]. Recently, *BCL6* was also identified to alleviate oxygen and glucose deprivation/reoxygenation induced cell inflammation damage and oxidative stress in IS [42]. Function analysis showed that *BCL6* was enriched in apoptosis and inflammation-related function, such as B cell apoptotic process, and mast cell cytokine production. Additionally, *BCL6* was predicted to be

regulated by miR-126-3p in the present study. The miR-126 plays a key role in the pathogenesis of IS and participates in endovascular inflammation [29,38]. Interestingly, *FCGR1A* was also regulated by miR-126-3p, and was involved in the pathway of immunoglobulin binding in this study. Immunoglobulin has been reported to protect brain cells against ischemic damage [7]. Both *ITGAM* and *TLR2* were regulated by miR-185-5p. miR-185 is one of miRNAs involved in angiogenesis in IS, and has been suggested to be a potential serum diagnostic indicator of neurological injury after IS [16,37]. Moreover, both *ITGAM* and *TLR2* were enriched in function associated with microglial cell activation.

Microglial cells are resident immune cells in the central nervous system, activation of which plays a central role in pathology of ischemic tissue, including IS [39]. Taken together, these model genes were associated with IS progression via some immune inflammation and apoptosis-related functions and pathways.

In conclusion, our study identified some immune-related marker genes and constructed a diagnostic model based on 8 immune-related genes in IS. Our results further suggested the critical role of immune and inflammation in IS. However, this study obtained some theoretical results only through the bioinformatics analysis, which need to be verified in clinical samples.

Funding

This research received no external funding.

Disclosures

Approval of the Bioethics Committee was not required.

The authors report no conflict of interest.

References

1. Ashburner M, Ball CA, Blake JA, Botstein D, Butler H, Cherry JM, Davis AP, Dolinski K, Dwight SS, Eppig JT. Gene ontology: tool for the unification of biology. Nat Genet 2000; 25: 25-29.
2. Barrett T, Suzek TO, Troup DB, Wilhite SE, Ngau W-C, Ledoux P, Rudnev D, Lash AE, Fujibuchi W, Edgar R. NCBI GEO: mining millions of expression profiles – database and tools. Nucleic Acids Res 2005; 33: D562-D566.
3. Bindea G, Mlecnik B, Hackl H, Charoentong P, Tosolini M, Kirilovsky A, Fridman WH, Pagès F, Trajanoski Z, Galon J. ClueGO: a Cytoscape plug-in to decipher functionally grouped gene ontology and pathway annotation networks. Bioinformatics 2009; 25: 1091-1093.
4. Chen B, Khodadoust MS, Liu CL, Newman AM, Alizadeh AA. Profiling tumor infiltrating immune cells with CIBERSORT. Methods Mol Biol 2018; 1711: 243-259.
5. Chen D, Xiong XQ, Zang YH, Tong Y, Zhou B, Chen Q, Li YH, Gao XY, Kang YM, Zhu GQ. BCL6 attenuates renal inflammation via negative regulation of NLRP3 transcription. Cell Death Dis 2017; 8: e3156-e3156.
6. Chu HX, Kim HA, Lee S, Moore JP, Chan CT, Vinh A, Gelderblom M, Arumugam TV, Broughton BR, Drummond GR. Immune cell infiltration in malignant middle cerebral artery infarction: comparison with transient cerebral ischemia. J Cereb Blood Flow Metab 2014; 34: 450-459.
7. D Fann Y-W, Lee S, Manzanero S, Tang S-C, Gelderblom M, Chunduri P, Bernreuther C, Glatzel M, Cheng Y-L, Thundyil J. Intravenous immunoglobulin suppresses NLRP1 and NLRP3 inflammasome-mediated neuronal death in ischemic stroke. Cell Death Dis 2013; 4: e790-e790.
8. Deb P, Sharma S, Hassan KM. Pathophysiologic mechanisms of acute ischemic stroke: An overview with emphasis on therapeutic significance beyond thrombolysis. Pathophysiology 2010; 17: 197-218.
9. Dziedzic T. Systemic inflammation as a therapeutic target in acute ischemic stroke. Expert Rev Neurother 2015; 15: 523-531.
10. Hasan TF, Rabinstein AA, Middlebrooks EH, Haranhalli N, Silliman SL, Meschia JF, Tawk RG. Diagnosis and management of acute ischemic stroke. Mayo Clin Proc 2018; 93: 523-538.
11. Iadecola C, Buckwalter MS, Anrather J. Immune responses to stroke: mechanisms, modulation, and therapeutic potential. J Clin Invest 2020; 130: 2777-2788.
12. Javidi E, Magnus T. Autoimmunity after ischemic stroke and brain injury. Front Immunol 2019; 10: 686.
13. Jayaraj RL, Azimullah S, Beiram R, Jalal FY, Rosenberg GA. Neuroinflammation: friend and foe for ischemic stroke. J Neuroinflammation 2019; 16: 142.
14. Jian Z, Liu R, Zhu X, Smerin D, Zhong Y, Gu L, Fang W, Xiong X. The involvement and therapy target of immune cells after ischemic stroke. Front Immunol 2019; 10: 2167.
15. Jiang B, Sun P, Tang J, Luo B. Glmnet: Graph learning-matching networks for feature matching. arXiv preprint arXiv:191107681, 2019.
16. Jin F, Xing J. Circulating pro-angiogenic and anti-angiogenic microRNA expressions in patients with acute ischemic stroke and their association with disease severity. Neurol Sci 2017; 38: 2015-2023.
17. Kanehisa M, Goto S. KEGG: Kyoto encyclopedia of genes and genomes. Nucleic Acids Res 2000; 28: 27-30.
18. Kawabori M, Yenari MA. Inflammatory responses in brain ischemia. Curr Med Chem 2015; 22: 1258-1277.
19. Kohl M, Wiese S, Warscheid B. Cytoscape: software for visualization and analysis of biological networks. Methods Mol Biol 2011; 696: 291-303.
20. Krishnan S, Lawrence CB. Old dog new tricks; revisiting how stroke modulates the systemic immune landscape. Front Neurol 2019; 10: 718.
21. Langfelder P, Horvath S. WGCNA: an R package for weighted correlation network analysis. BMC Bioinformatics 2008; 9: 1-13.
22. Laskowitz DT, Kasner SE, Saver J, Remmel KS, Jauch EC. Clinical usefulness of a biomarker-based diagnostic test for acute stroke: the Biomarker Rapid Assessment in Ischemic Injury (BRAIN) study. Stroke 2009; 40: 77-85.
23. Lo EH, Dalkara T, Moskowitz MA. Mechanisms, challenges and opportunities in stroke. Nat Rev Neurosci 2003; 4: 399-415.
24. Lu P, Chen J, Zhao H, Gao Y, Luo L, Zuo X, Shi Q, Yang Y, Yi J, Wang W. In silico syndrome prediction for coronary artery disease in traditional Chinese medicine. Evid Based Complement Alternat Med 2012; 2012: 142584.
25. Ma Y, Yabluchanskiy A, Iyer RP, Cannon PL, Flynn ER, Jung M, Henry J, Cates CA, Deleon-Pennell KY, Lindsey ML. Temporal

neutrophil polarization following myocardial infarction. Cardiovasc Res 2016; 110: 51-61.
26. Maida CD, Norrito RL, Daidone M, Tuttolomondo A, Pinto A. Neuroinflammatory mechanisms in ischemic stroke: focus on cardioembolic stroke, background, and therapeutic approaches. Int J Mol Sci 2020; 21: 6454.
27. Mering C, Huynen M, Jaeggi D, Schmidt S, Bork P, Snel B. STRING: a database of predicted functional associations between proteins. Nucleic Acids Res 2003; 31: 258-261.
28. Radak D, Katsiki N, Resanovic I, Jovanovic A, Sudar-Milovanovic E, Zafirovic S, Mousad SA, R Isenovic E. Apoptosis and acute brain ischemia in ischemic stroke. Curr Vasc Pharmacol 2017; 15: 115-122.
29. Schober A, Nazari-Jahantigh M, Wei Y, Bidzhekov K, Gremse F, Grommes J, Megens RT, Heyll K, Noels H, Hristov M. MicroRNA-126-5p promotes endothelial proliferation and limits atherosclerosis by suppressing Dlk1. Nat Med 2014; 20: 368-376.
30. Sherman BT, Hao M, Qiu J, Jiao X, Baseler MW, Lane HC, Imamichi T, Chang W. DAVID: a web server for functional enrichment analysis and functional annotation of gene lists (2021 update). Nucleic Acids Res 2022; 50: W216-W221.
31. Smyth GK, Ritchie M, Thorne N, Wettenhall J. LIMMA: linear models for microarray data. In: Bioinformatics and Computational Biology Solutions Using R and Bioconductor. Statistics for Biology and Health, 2005.
32. Sticht C, De La Torre C, Parveen A, Gretz N. miRWalk: an online resource for prediction of microRNA binding sites. PLoS One 2018; 13: e0206239.
33. Stubbe T, Ebner F, Richter D, Engel OR, Klehmet J, Royl G, Meisel A, Nitsch R, Meisel C, Brandt C. Regulatory T cells accumulate and proliferate in the ischemic hemisphere for up to 30 days after MCAO. J Cereb Blood Flow Metab 2013; 33: 37-47.
34. Tang Y, Li M, Wang J, Pan Y, Wu FX. CytoNCA: a cytoscape plugin for centrality analysis and evaluation of protein interaction networks. Biosystems 2015; 127: 67-72.
35. Tuttolomondo A, Pinto A, Corrao S, Di Raimondo D, Fernandez P, Di Sciacca R, Arnao V, Licata G. Immuno-inflammatory and thrombotic/fibrinolytic variables associated with acute ischemic stroke diagnosis. Atherosclerosis 2009; 203: 503-508.
36. Uemura Y, Kowall NW, Moskowitz MA. Focal ischemia in rats causes time-dependent expression of c-fos protein immunoreactivity in widespread regions of ipsilateral cortex. Brain Res 1991; 552: 99-105.
37. Wang R, Bao H, Zhang S, Li R, Chen L, Zhu Y. miR-186-5p promotes apoptosis by targeting IGF-1 in SH-SY5Y OGD/R model. Int J Biol Sci 2018; 14: 1791-1799.
38. Wei X, Han M, Yang F, Wei G, Liang Z, Yao H, Ji C, Xie R, Gong C, Tian Y. Biological significance of miR-126 expression in atrial fibrillation and heart failure. Braz J Med Biol Res 2015; 48: 983-989.
39. Zhang S. Microglial activation after ischaemic stroke. Stroke Vasc Neurol 2019; 4: 71-74.
40. Zhang SR, Phan TG, Sobey CG. Targeting the Immune System for Ischemic Stroke. Trends Pharmacol Sci 2021; 42: 96-105.
41. Zheng Y, Gardner SE, Clarke MC. Cell death, damage-associated molecular patterns, and sterile inflammation in cardiovascular disease. Arterioscler Thromb Vasc Biol 2011; 31: 2781-2786.
42. Zhou ZW, Ren X, Zhou WS, Li AP, Zheng LJ. LncRNA NEAT1 alleviates ischemic stroke via transcriptional inhibition of NLRP3 mediated by the miR-10b-5p/BCL6 axis. Acta Neurobiol Exp (Wars) 2022; 82: 12-21.